Journal of Applied Polymer Science

Crystallization and Mechanical Properties of Isotactic Polypropylene/Calcium Carbonate Nanocomposites with a Stratified Distribution of Calcium Carbonate

Ming Wang,[1] Lu Lin,[1] Qicai Peng,[1] Wenyong Ou,[1] Huilin Li[2]

[1]School of Chemistry and Chemical Engineering, Southwest University, Chongqing 400715, China

[2]State Key Laboratory of Polymer Materials Engineering, Polymer Research Institute of Sichuan University, Chengdu 610065, China

Correspondence to: M. Wang (E-mail: mwang@swu.edu.cn)

ABSTRACT: Isotactic polypropylene (iPP)/calcium carbonate ($CaCO_3$) nanocomposites with a stratified distribution of $CaCO_3$ were prepared by two-step molding. The iPP and $CaCO_3$ nanoparticles were first mixed by a batch mixer and then compressed into thin layers. Thin iPP/$CaCO_3$ layers alternating with thin neat iPP layers were finally compressed together to form the stratified samples. The transcrystals were observed in the stratified samples by polarized optical microscopy and scanning electron microscopy. The transcrystals grew from the surfaces of the filled layers and occupied most of the space in the neat iPP layers. The β-form crystals were found in the stratified samples with thick transcrystalline layers, whereas the thickness of the transcrystalline layer was dependent on the content of $CaCO_3$ nanoparticles and the cooling rate of the processing. The relative crystallinity index of the conventional samples first increased and then decreased with the content of $CaCO_3$ nanoparticles. However, the relative crystallinity index of the stratified samples deceased slightly with the content of $CaCO_3$ nanoparticles because of the stratified distribution of the $CaCO_3$ nanoparticles. The stratified samples, except for the samples with high β-form contents, became more brittle than the conventional samples because of the transcrystal formation in the iPP layers. The stratified samples with high β-form contents showed much better mechanical properties than the conventional samples. © 2013 Wiley Periodicals, Inc. J. Appl. Polym. Sci. **2014**, *131*, 39632.

KEYWORDS: composites; crystallization; morphology

Received 21 March 2013; accepted 6 June 2013

DOI: 10.1002/app.39632

INTRODUCTION

The development of polymer nanocomposites can be regarded as a significant technological advancement in both the academic and industrial areas in recent years. An important issue in the processing of polymer nanocomposites is the morphological control of the matrix materials. Morphological features, such as the degree of crystallinity, crystalline morphology, spherulite size, lamellar thickness, and crystal orientation, can all have a dominant effect on the ultimate properties of the polymer matrix and, hence, on the composites. It is now well-known that the existence of a foreign surface can alter the crystallization behavior, such as the crystalline structure and morphology, of a polymer and, therefore, provide an efficient way to fabricate special structures with desired properties.[1]

Polymer/calcium carbonate ($CaCO_3$) nanocomposites are one kind of famous composites in normal use. Polypropylene (PP) is extensively used in automobile and electronic appliance applications because of its good performance, processing properties, and low cost. Calcium carbonate is one of the most commonly used fillers in thermoplastics, especially for polyolefin. In most cases, $CaCO_3$ nanoparticle can significantly enhance the tensile strength, Young's modulus, and dimensional stability, but it decreases the toughness for many polymers.[2–4] Recently, it was reported that both the stiffness and toughness of polymers could be increased by the addition of well dispersed or modified $CaCO_3$ nanoparticles.[5–10] This topic has attracted much interest in the scientific field because of the possibility of using low contents of fillers for great increases in both the impact and tensile mechanical properties. However, their practical application as structural reinforcing fillers critically depends on the effective interfacial load transfer from the polymer matrix to the particles. In semicrystalline polymers, the interfacial supramolecular structure induced by the particles plays a crucial role in enhancing the load transfer. $CaCO_3$ particles are normally used to reinforce polymers and act as heterogeneous nucleating agents for polymer crystallization along the interface.[11] The spherulite size of PP decreases with the addition of $CaCO_3$ particles, and β crystals can form in composites with $CaCO_3$ particles.[12]

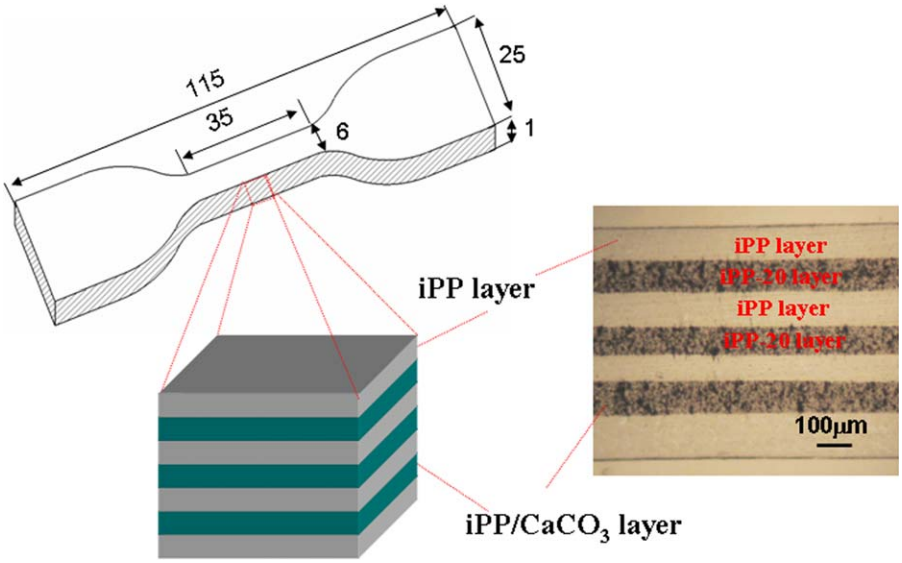

Figure 1. Schematic drawing of the shape and dimension of the iPP/$CaCO_3$ nanocomposites with $CaCO_3$ stratified distribution for tensile. The right side shows the optical micrograph of the iPP/iPP-20 sample including three iPP-20 layers (layers with black particles) and four neat iPP layers (transparent layers). [Color figure can be viewed in the online issue, which is available at wileyonlinelibrary.com.]

Transcrystals are well-known structural features in polymers; they occur as the result of overgrowth of polymer crystals on organic and inorganic fibers.[1,13–17] In this case, heterogeneous nucleation occurs with a high density of active nuclei at the fiber surface, and then, the crystal growth is restricted to the lateral direction so that a columnar layer develops around the fiber. Transcrystallization is a nucleation-controlled process, and the enhanced nucleation at the fiber surface is the key factor in the formation of a transcrystalline morphology.[14] This type of directional crystal growth can yield substantial molecular orientation within the transcrystalline layers and thus influence the mechanical properties of the material.[15–17] Many researchers have reported that polymers with transcrystals were stiff and brittle in comparison with the fine spherulitic polymers; this probably gave rise to a high Young's modulus, adhesion, shear, and tensile yield strengths in the transcrystalline composites.[18–22] However, previous studies concerning transcrystallized polymer materials have generally focused on fiber composites or model systems. The shape of $CaCO_3$ particles is spherical. They are usually defined as zero-dimension (0D) particles. To the best of our knowledge, there has been no report showing obvious transcrystals in polymer/0D particles. Baer and Hiltner and coworkers prepared stratified distribution fillers in polymers by multilayered coextrusion[23–25] and also studied the effect of dimension confinement on polymer crystallization.[26–28] However, transcrystals in these kinds of polymer composites were not mentioned.

In this article, we show clear-cut evidence that the transcrystallization of isotactic polypropylene (iPP) could also take place in polymer/0D particle ($CaCO_3$ in this study) composites with a stratified distribution of particles, instead of only spherulites. We also tried to further enhance the mechanical properties of the $CaCO_3$-filled polymer materials incorporated with the transcrystals. The crystalline morphology, including transcrystals, were investigated to uncover the essential contributions for the properties of the nanocomposites.

EXPERIMENTAL

Materials

A commercially available iPP was manufactured by Lanzhou Petroleum Chemical, Inc. (Gansu, China), with a melt flow index of 2.5 g/10 min (190°C, 2.16 kg) and a density of 0.90–0.91 g/cm^3. $CaCO_3$ nanoparticles with an average diameter of 55 nm were produced by Jiangxi Jingxue Co. (Jiangxi, China).

Sample Preparation

Conventional iPP/$CaCO_3$ Nanocomposites. The conventional iPP/$CaCO_3$ nanocomposites with 2.5, 5, 10, 20, and 50 wt % $CaCO_3$ content were melt-mixed in a batch mixer to comparatively study the transcrystalline effect on the mechanical properties. The mixing time was set at 5 min. The temperature was set at 200°C. After melt-mixing, the conventional iPP/$CaCO_3$ nanocomposites were molded in a rectangle shape 1 mm in thickness by compression molding with a 10-MPa press at 200°C to tailor the tensile samples.

Stratified iPP/$CaCO_3$ Nanocomposites. First, three thin films of iPP/$CaCO_3$ nanocomposites with 5, 10, 20, or 50 wt % $CaCO_3$ contents and 0.15 mm thicknesses were prepared by conventional compression molding under 10 MPa of stress at 200°C. Four thin films of neat iPP with 0.15 mm thicknesses were also molded under 10 MPa of stress at 200°C. Second, the previous seven films were alternately sandwiched with iPP films at the surface and then compressed under 10 MPa of stress at 200°C to form the final composites, which were 1 mm thick, as shown in Figure 1. As a result, the total content of $CaCO_3$ particles in these stratified samples was close to half of the iPP/$CaCO_3$ layers within. Before sandwiching, all of the thin films were washed with alcohol to make there was sure no dust

Table I. Abbreviations for the Samples Used in This Study

Sample	Description
iPP-2.5	Conventional blends with 2.5 wt % $CaCO_3$
iPP-5	Conventional blends with 5 wt % $CaCO_3$
iPP-10	Conventional blends with 10 wt % $CaCO_3$
iPP-20	Conventional blends with 20 wt % $CaCO_3$
iPP-50	Conventional blends with 50 wt % $CaCO_3$
iPP/iPP-5	Seven-layer composites, iPP/$CaCO_3$ layers with 5 wt % $CaCO_3$
iPP/iPP-10	Seven-layer composites, iPP/$CaCO_3$ layers with 10 wt % $CaCO_3$
iPP/iPP-20	Seven-layer composites, iPP/$CaCO_3$ layers with 20 wt % $CaCO_3$
iPP/iPP-50	Seven-layer composites, iPP/$CaCO_3$ layers with 50 wt % $CaCO_3$

on the surfaces. Finally, iPP/$CaCO_3$ nanocomposites with a stratified distribution of $CaCO_3$ were successfully prepared by this two-step molding. The $CaCO_3$ nanoparticles were dispersed in a constrained manner in the iPP/$CaCO_3$ layers. The optical micrograph in Figure 1 shows that no layer was broken, and the clear interfaces were maintained. The thickness of the thin films near the surface was thicker than that at the center because of the expansion after stress release from the surface. A series of conventional and stratified samples were prepared, and the abbreviations of the samples used in this study are shown in Table I.

Measurements

Polarized Optical Microscopy (POM). The $CaCO_3$ dispersion and the transcrystalline morphology of the samples were investigated by POM (Olympus, BX51-P). A slice 15 μm thick was cryogenically microtomed from the nanocomposites in the thickness direction for the observation.

Differential Scanning Calorimetry (DSC). The crystalline characteristics of the nanocomposites were studied by DSC (TA DSC 204) with nitrogen as a purge gas. The nonisothermal crystalline melting behavior of the specimens was obtained through the melting of the samples (ca. 5 mg) from 25°C at a heating rate of 10°C/min. To study effect of the cooling rate on the crystalline behavior, the samples were melted at 220°C for 5 min to remove any thermal history and then cooled to 25°C at 10, 5, and 3°C/min. Finally, they were heated to 220°C at a heating rate of 10°C/min.

X-ray Diffraction (XRD). Wide-angle XRD analysis was performed on a MSAL-XD 3 (Beijing Purkinje General Instrument Co., Ltd., China) with Cu Kα radiation with a wavelength of 1.54 Å (36 kV and 20 mA). Scanning was performed over the angle range $2\theta = 10$–40° at a scanning rate of 4°/min. The β-form content (K_β) was calculated by the Turner–Jones's equation as follows:[29]

$$K_\beta = \frac{I_{\beta(300)}}{I_{\beta(300)} + I_{\alpha(110)} + I_{\alpha(040)} + I_{\alpha(130)}} \quad (1)$$

where $I_{\beta(300)}$ is the intensity of the characteristic peak of the β-form crystals and $I_{\alpha(110)}$, $I_{\alpha(040)}$, and $I_{\alpha(130)}$ are the intensities of the characteristic peaks of the α crystals.

Scanning Electron Microscopy (SEM). The $CaCO_3$ dispersion in the samples was also characterized by an S3000N Hitachi scanning electron microscope at 20 kV. The samples were first cryogenically fractured in liquid nitrogen and then coated with a thin layer of gold before the observation. To investigate the crystalline morphology, the cryogenically fractured samples were etched by a 1% solution of potassium permanganate a 10:4:1 v/v mixture of concentrated sulfuric acid, 85% orthophosphoric acid, and water to remove the amorphous part of iPP.[30] To observe the fracture behavior of the samples, the tensile fracture surfaces of the samples were directly coated with gold and then examined by SEM.

Tensile Experiments. Tensile tests were performed with an Instron universal tensile testing machine with a crosshead speed of 20 mm/min. The measured temperature was set at 23 ± 2°C. The average values from at least five samples were reported.

RESULTS AND DISCUSSION

Crystalline Morphology and Crystallization Behavior in the Stratified Nanocomposites

Figure 2(a) shows that the crystalline morphologies of the iPP layers were very different from those of the filled iPP layers in the stratified samples. Because of the nucleating effect of the $CaCO_3$ nanoparticles, the size of the crystals in the filled iPP layers was smaller than that in the iPP layers. In addition to the spherulites, transcrystals were found in the iPP layers. The transcrystals grew from the interfaces and acted act as fibers with a high density of active nuclei. In kinetics, the $CaCO_3$ nanoparticles increased the peak temperature of crystallization, and the crystallization rate of iPP because of the nucleation effect of the $CaCO_3$ nanoparticles.[31,32] As a result, crystallization first occurred at the interfaces to form transcrystals in the iPP layers, and the spherulites subsequently appeared in the center of the iPP layers. The final crystalline morphology of the iPP layers was transcrystalline at the interfaces and spherulitic in the center. The SEM images further proved the crystalline morphology in the iPP layers. The crystalline domains were unfolded by the etching of the amorphous phase. The $CaCO_3$ nanoparticles were also etched by the solution, and the holes were clear in the iPP/$CaCO_3$ layers. Big holes indicated the aggregation of $CaCO_3$ nanoparticles [Figure 2(b)]. To clearly show the two different crystals, the etched surface with high magnification are shown in Figure 2(c). The two black lines indicate the interfaces of the spherulites and the transcrystals.

We found that the transcrystalline thickness in the iPP layer was relative to the content of $CaCO_3$ nanoparticles in the nearby iPP/$CaCO_3$ layer. Figure 3 shows the transcrystalline thickness, which was from the interface of the iPP layer and the iPP/$CaCO_3$ layer to the interface of the transcrystal, and the spherulite decreased with $CaCO_3$ nanoparticle content. The iPP/iPP-5 samples had the thickest transcrystals (ca. 83 μm), which

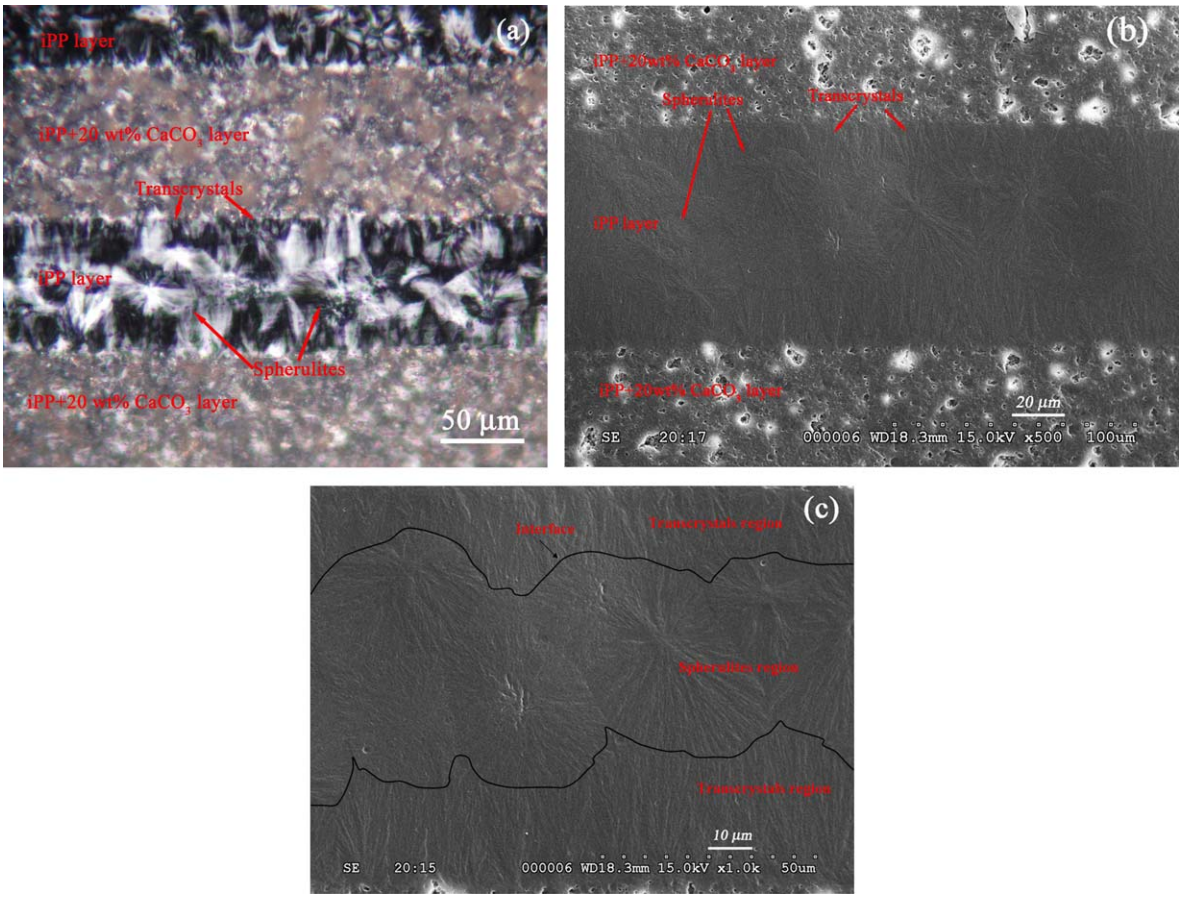

Figure 2. (a) POM image and (b,c) SEM micrographs representing the transcrystallization at the interfaces of the iPP layers and iPP-20 layers. [Color figure can be viewed in the online issue, which is available at wileyonlinelibrary.com.]

occupied the whole iPP layers. The thickness of the transcrystals in the iPP/iPP-50 samples was about 16 μm; this was the thinnest in the stratified samples. These results indicate that the density of the nucleating point on the composite layer merely influenced the compactness of transcrystallization, but it did not determine the growth rate of the transcrystalline layer. The number of transcrystalline nucleating points increased with the content of $CaCO_3$ nanoparticles at the interfaces. More

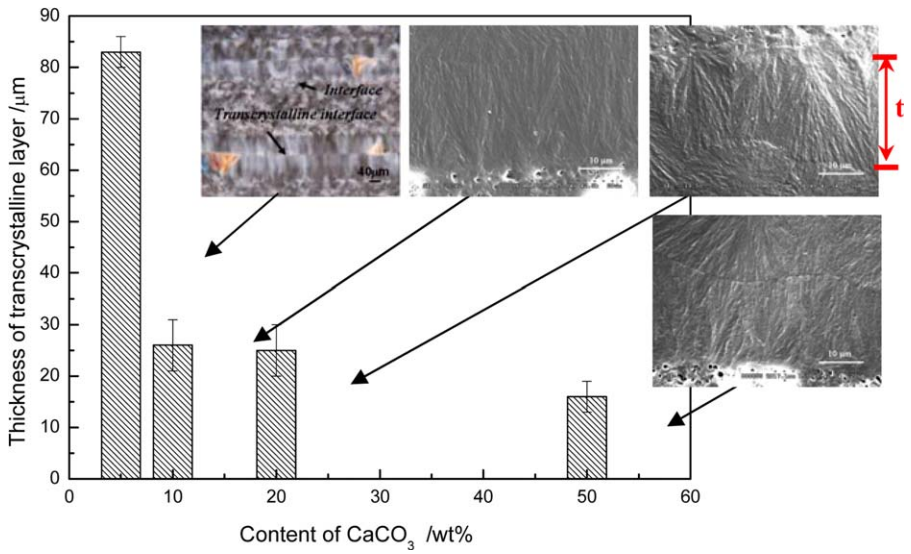

Figure 3. Effect of the $CaCO_3$ content in the iPP/$CaCO_3$ layers on the transcrystalline thickness in the iPP layers. [Color figure can be viewed in the online issue, which is available at wileyonlinelibrary.com.]

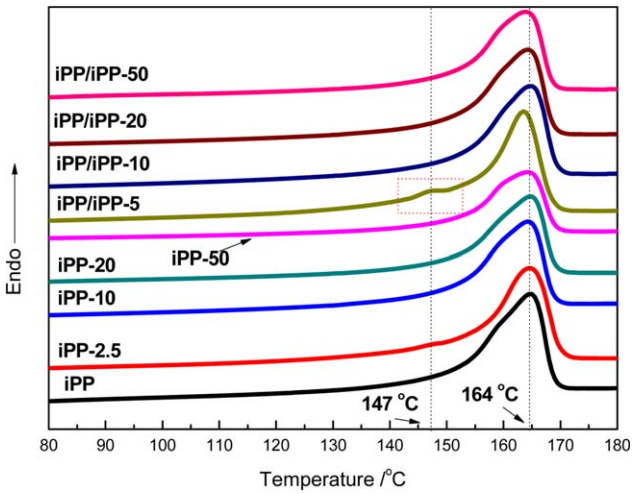

Figure 4. Comparison of the melting curves of the iPP/$CaCO_3$ nanocomposites at the first melting with a heating rate of 10°C/min. [Color figure can be viewed in the online issue, which is available at wileyonlinelibrary.com.]

crystalline nuclei made the transcrystals smaller at the same crystallization conditions because of the confined space.

The nonisothermal crystallization and melting behavior was investigated by DSC analysis. Figure 4 shows the melting curves of the iPP and iPP/$CaCO_3$ nanocomposites at first melting with a heating rate of 10°C/min. All of the samples, including the stratified samples and except for the iPP/iPP-5 samples, had only one melting temperature of the iPP α-form crystals (164°C). The XRD results also show that there was no β-form crystal (⟨300⟩, characteristic peak of β-form crystals) in any of the samples expect for the iPP/iPP-5 samples (Figure 5). A small melting peak of the β-form crystal at 147°C was found in the iPP/iPP-5 samples, which had the thickest transcrystalline layers. The results indicate that the β-form crystals probably preferred to form in thick transcrystalline layers. The ratio of the height of the melting peak of the α-form crystals to that of the β-form crystals (R) was

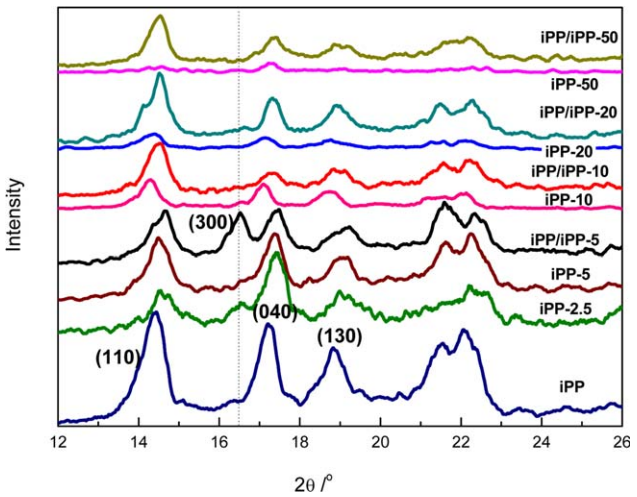

Figure 5. XRD results of the iPP and the iPP/nano-$CaCO_3$ nanocomposites. [Color figure can be viewed in the online issue, which is available at wileyonlinelibrary.com.]

about 0.18, as shown in Figure 4. The β-form content was 15%; this was very close to the value calculated by eq. (1) from the XRD results shown in Figure 5. It must be pointed out that the first melting curve was dependent on the thermal history of the processing. All of the samples were prepared by compression molding, and the cooling rate was about 50°C/min. That was a very rapid cooling rate. We predict that the β-form content would increase when the cooling rate is slowed because the thickness of the transcrystals would probably increase as well.

Figure 6 shows the melting curves of the samples under a cooling rate of 10, 5, and 3°C/min, respectively. The intensity of the melting peak of the β-form crystals was enhanced when the cooling rate was decreased. The β-form content increased when the cooling rate was slowed. R was calculated. Here, we must point out that the R value just provides a semiquantitative analysis compared to the K_β value from eq. (1). Table II shows the R value of the samples at different cooling rates. The results indicate that the β-form crystals could be easily formed in the stratified samples at the low cooling rate. In the iPP/iPP-5 sample, for example, the ratio that went up to 0.45 at a cooling rate of 3°C/min was 0.18 at a cooling rate of about 50°C/min. It was reported that the β-form crystals were related to the crystallization temperature dependence. The rate of α-form crystals was larger at higher and lower crystallization temperatures, and the rate of β-form crystals was larger at the middle temperature.[33,34] The low cooling rate provided a long crystallization time for the β-form crystallization at the middle temperature.

The formation of β-form crystals was not only related to the cooling rate but also dependent on the content of $CaCO_3$ nanoparticles. The samples with lower $CaCO_3$ contents had higher β-form contents. Thus, the iPP/iPP-5 samples had the highest density of the β-form crystals in all of the samples at a cooling rate of 3°C/min. In the literature, it was shown that β-form crystals could be formed under some special conditions, such as with the addition of a β-nucleating agent,[35–44] directional crystallization at certain temperature gradients,[45] and shearing or elongation of the melt during crystallization.[46–50] In our case, the nearby polymer chains were oriented by the transcrystalline crystallization of the polymer chains for the first. The oriented chains probably formed β nuclei and then β-form crystals formed. The samples with thick transcrystals had greater opportunities to crystallize the β-form crystals than the samples with thin transcrystals. Second, the ratio of β-form-crystal to α-form-crystal contents was relative to the content of nucleating agents. The low concentration produced a high β-form percentage.[35–40] Thus, the high β-form content was found in the stratified samples with low contents of $CaCO_3$ at a slow cooling rate because of the thick transcrystalline layer that formed in that situation.

Effect of the Transcrystals on the Mechanical Properties of the Nanocomposites

Figure 7 shows the mechanical properties of the iPP/$CaCO_3$ nanocomposites. The mechanical properties of the iPP/$CaCO_3$ samples were relative to the distribution and content of the $CaCO_3$ nanoparticles. For the conventional blends, the Young's modulus increased and the strain at break decreased with the content of $CaCO_3$ nanoparticles. The yield strength of the conventional

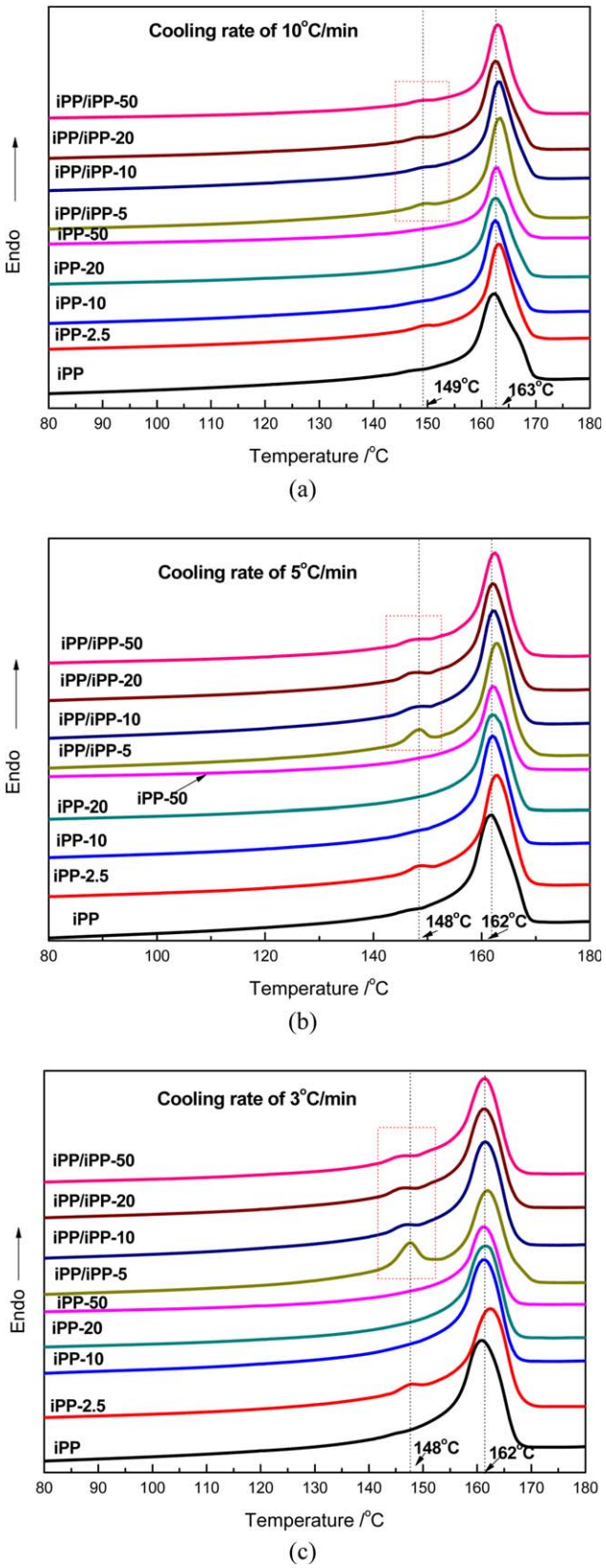

Figure 6. Comparison of the melting curves of the iPP/$CaCO_3$ nanocomposites treated at different cooling rates: (a) 10, (b) 5, and (c) 3°C/min and with a heating rate of 10°C/min. [Color figure can be viewed in the online issue, which is available at wileyonlinelibrary.com.]

blends first increased with the content of $CaCO_3$ nanoparticles and then decreased when the content of $CaCO_3$ nanoparticles was above 5 wt %. These results indicate that the nanoparticles made the iPP matrix brittle and less tough. The aggregation of the nanoparticles, which produced remarkable stress concentration, further decreased the toughness of the iPP. The degree of aggregation increased with the content of $CaCO_3$ nanoparticles. The yield strength first increased from about 25 MPa for neat iPP to about 27 MPa for the iPP-5 nanocomposites and then decreased to about 21 MPa of the iPP-50 nanocomposites. The variation of the yield strength was ascribed to the variation of the relative crystallinity index in the iPP/$CaCO_3$ nanocomposites. Hong and Strobl[51] also reported that yield strength increased with crystallinity in semicrystalline polymers. The insets in Figure 7(c) show that the relative crystallinity index of the conventional composites also first increased with the content of $CaCO_3$ nanoparticles and then decreased when the content of $CaCO_3$ nanoparticles was above 5 wt %. Because of the nucleating effect, the relative crystallinity index of the samples increased when the content of $CaCO_3$ nanoparticles was low. However, the relative crystallinity index decreased in the highly filled samples because of the movement of polymer chains confined by the overfull nanoparticles and also the low content of iPP.

For the stratified samples, the Young's modulus also increased and the strain at break also decreased with the content of $CaCO_3$ nanoparticles. However, the stratified samples, except for the iPP/iPP-5 samples, had a higher Young's modulus and lower strain at break than that of the conventional samples with close contents of $CaCO_3$ nanoparticles. For examples, the iPP-5 and iPP/iPP-10 samples had close contents of $CaCO_3$ nanoparticles, but the Young's modulus of the iPP/iPP-10 samples was 23% higher and the strain at break was 68% lower than those of the iPP-5 samples. The results indicate that the stratified samples were more brittle than the conventional samples. We believe that the brittle enhancement was related to the transcrystals in the iPP layers because the transcrystals were stiff and brittle in comparison with the fine spherulites.[14] Figure 7(c) shows that the yield strength of the stratified samples slightly decreased with the content of $CaCO_3$ nanoparticles because their relative crystallinity index slightly decreased as well. Interestingly, the mechanical properties, especially the strain at break, of the iPP/iPP-5 samples were higher

Table II. *R* Values in the Composites at Different Cooling Rates

Sample	*R*(50)	*R*(10)	*R*(5)	*R*(3)
iPP	0	0	0	0
iPP-2.5	0	0.15	0.18	0.23
iPP-10	0	0	0	0
iPP-20	0	0	0	0
iPP-50	0	0	0	0
iPP/iPP-5	0.18	0.20	0.23	0.45
iPP/iPP-10	0	0.13	0.17	0.21
iPP/iPP-20	0	0.12	0.16	0.20
iPP/iPP-50	0	0.12	0.15	0.18

R represents the ratio, and the number in parentheses is the cooling rate.

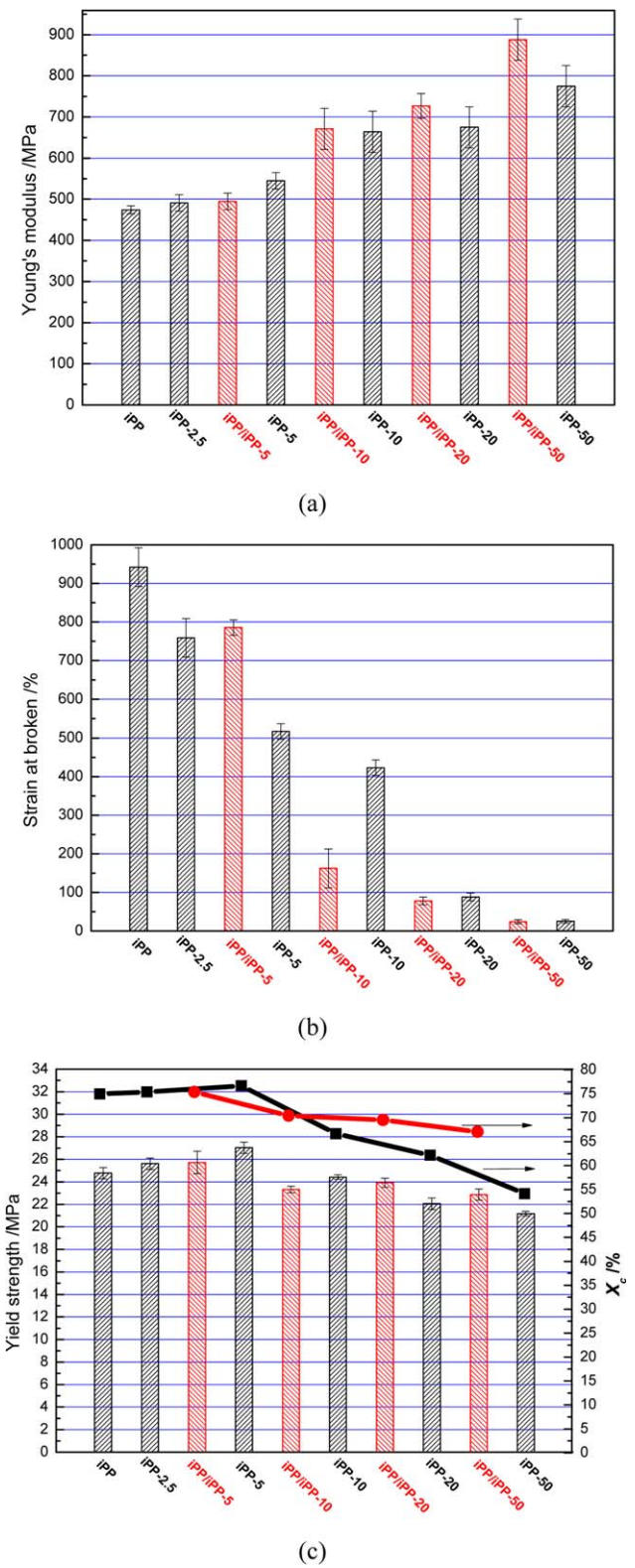

Figure 7. (a) Young's modulus, (b) strain at break, and (c) yield strength of the iPP/$CaCO_3$ nanocomposites. The inset symbol and line in part c shows the relative crystallinity index (X_c) of the iPP/$CaCO_3$ nanocomposites calculated from the XRD results in Figure 5. [Color figure can be viewed in the online issue, which is available at wileyonlinelibrary.com.]

than those of the iPP-2.5 samples. This was ascribed to the high β-form content of the iPP/iPP-5 samples. The β-form crystals had a higher ductility and strength than that of the α-form crystals with little loss of stiffness.[34]

Figure 8 shows the SEM images of the tensile fracture surfaces in the conventional and stratified samples. Figure 8(a–d) presents the fracture surfaces of the iPP-5, iPP-10, iPP-20, and iPP-50 samples, respectively. The rough fracture surfaces of the iPP-5, iPP-10, and iPP-20 samples indicated the polymer chains pulling out and the tough fracture happening in these stretched samples. However, stiff fracture occurred in the iPP-50 samples because of the relatively smooth fracture surface and lots of aggregated $CaCO_3$ nanoparticles therein. The aggregated $CaCO_3$ nanoparticles, providing stress concentration, made the composites become brittle.

The facture surfaces of the stratified samples were very different from that of the conventional samples. The pure iPP layers and the $CaCO_3$ filled iPP layers exhibited different fracture behaviors. Figure 8(e–h) presents the fracture surfaces of the iPP/iPP-5, iPP/iPP-10, iPP/iPP-20, and iPP/iPP-50 samples, respectively. The fracture surfaces of the pure iPP layers were much smoother than the fracture surfaces of the filled iPP layers in the iPP/iPP-5, iPP/iPP-10, and iPP/iPP-20 samples. These results indicate that stiff facture occurred in the iPP layers and tough fracture occurred in the filled iPP layers. Generally speaking, the neat iPP exhibited tough behavior under tensile stress. However, it became brittle in the stratified samples. This was ascribed to the transcrystals at the iPP layers in the stratified samples. The transcrystals, which were formed in the iPP layers by the nucleation of the nearby filled iPP layers, were stiff and brittle.

CONCLUSIONS

The transcrystals were successfully fabricated in the iPP/$CaCO_3$ nanocomposites through control of the distribution of $CaCO_3$ nanoparticles. The transcrystals were found in the iPP layers in the stratified samples. The thickness of the transcrystalline layer was dependent on the content of $CaCO_3$ nanoparticles. The thick transcrystalline layers were found in the low content of $CaCO_3$ nanoparticles. The β-form crystals could easily form in the stratified samples with thick transcrystalline layers because of the oriented polymer chains formed by the formation of the transcrystals. The low cooling rate was beneficial to the formation of the β-form crystals because of the formation of the thick transcrystalline layers and the long crystallization time for the β-form crystallization. Both the conventional samples and the stratified samples became stiff and brittle with the addition of $CaCO_3$ nanoparticles. The Young's modulus increased and the strain at break decreased with the $CaCO_3$ nanoparticles. Because of the transcrystals in the iPP layers, the stratified samples, except for the samples with high β-form crystals, exhibited more brittleness than the conventional samples. The fracture surfaces of the iPP layer exhibited stiff behavior in the stratified samples. The yield strength, which was affected by the relative crystallinity index, first increased and then decreased when the content of $CaCO_3$ nanoparticles was above 5 wt % for the conventional samples and slightly decreased for the stratified samples. The stratified samples

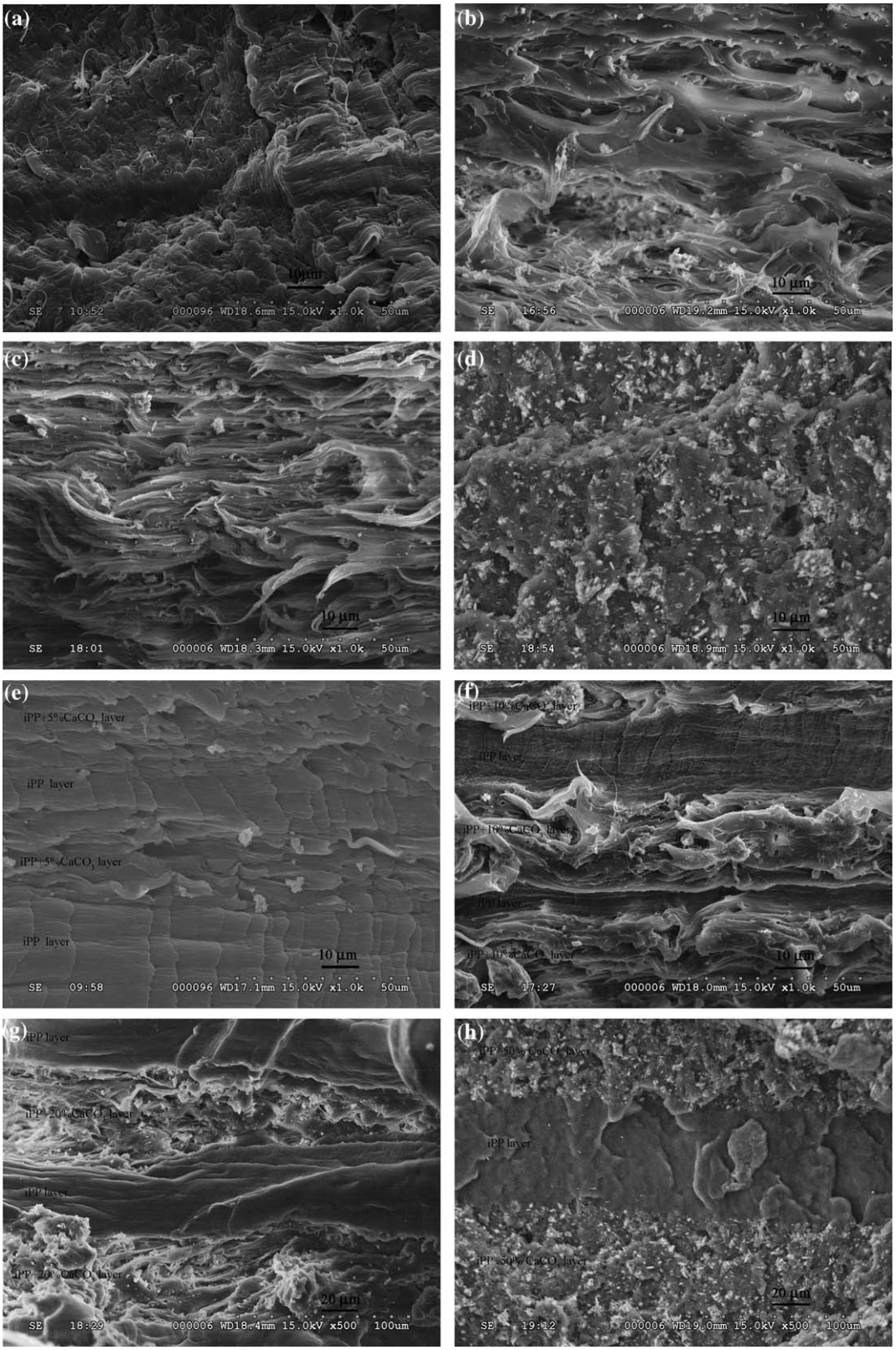

Figure 8. Scanning electron micrographs of the tensile fracture surfaces of the iPP/$CaCO_3$ nanocomposites: (a) iPP-5, (b) iPP-10, (c) iPP-20, (d) iPP-50, (e) iPP/iPP-5, (f) iPP/iPP-10, (g) iPP/iPP-20, and (h) iPP/iPP-50.

with high β-form contents showed much better mechanical properties than the corresponding conventional samples.

ACKNOWLEDGMENTS

The authors are grateful to the National Natural Science Foundation of China (contract grant number 51103119), the Opening Project of the State Key Laboratory of Polymer Materials Engineering of Sichuan University (contract grant number KF200905), the Natural Science Foundation Project of ChongQing (contract grant number CSTC 2010BB4009), the Doctor Founding of Southwest University (contract grant number SWU109024), and the Fundamental Research Funds for Central Universities (contract grant number XDJK2010C008) for their financial support of this work and Professor Guo's group at the State Key Laboratory of Polymer Materials Engineering for providing the DSC and POM tests in this study.

REFERENCES

1. Li, H.; Yan, S. *Macromolecules* **2011**, *44*, 417.
2. Mitsuishi, K.; Kodama, S.; Kawasaki, H. *Polym. Eng. Sci.* **1985**, *25*, 1069.
3. Eiras, D.; Pessan, L. A. *Mater. Res.* **2009**, *12*, 517.
4. Chan, C. M.; Wu, J.; Li, J. X.; Cheung, Y. K. *Polymer* **2002**, *43*, 2981.
5. Zuiderduin, W. C. J.; Westzaan, C.; Huétink, J.; Gaymans, R. *J. Polymer* **2003**, *44*, 261.
6. Lin, Y.; Chen, H.; Chan, C. M.; Wu, J. *Polymer* **2010**, *51*, 3277.
7. Lin, Y.; Chen, H.; Chan, C. M.; Wu, J. *Macromolecules* **2008**, *41*, 9204.
8. Fuad, M. Y. A.; Hanim, H.; Zarina, R.; Mohd Ishak, Z. A.; Hassan, A. *Express Polym. Lett.* **2010**, *4*, 611.
9. Etelaho, P.; Haveri, S.; Jrvel, P. *Polym. Compos.* **2011**, *32*, 464.
10. Zhang, J.; Han, B.; Zhou, N. L.; Fang, J.; Wu, J.; Ma, Z. M.; Mo, H.; Shen, J. *J. Appl. Polym. Sci.* **2011**, *119*, 3560.
11. Lin, Y.; Chen, H.; Chan, C. M.; Wu, J. *J. Colloid Interface Sci.* **2011**, *354*, 570.
12. Labour, T.; Vigier, G.; Séguéla, R.; Gauthier, C.; Orange, G.; Bomal, Y. *J. Polym. Sci. Part B: Polym. Phys.* **2002**, *40*, 31.
13. Keller, A. *J. Polym. Sci.* **1955**, *15*, 31.
14. Folkes, M. J.; Hardwick, S. T. *J. Mater. Sci. Lett.* **1987**, *6*, 656.
15. Li, Z. M.; Li, L. B.; Shen, K. Z.; Yang, W.; Huang, R.; Yang, M.-B. *Macromol. Rapid Commun.* **2004**, *25*, 553.
16. Wang, K.; Guo, M.; Zhao, D.; Zhang, Q.; Du, R.; Fu, Q.; Dong, X.; Han, C. C. *Polymer* **2006**, *47*, 8374.
17. Garkhail, S.; Wieland, B.; George, J.; Soykeabkaew, N.; Peijs, T. *J. Mater. Sci.* **2009**, *44*, 510.
18. Cho, K.; Kim, D.; Yoon, S. *Macromolecules* **2003**, *36*, 7652.
19. Lee, B. G.; Lee, S.; Via, B. K. *J. Appl. Polym. Sci.* **2010**, *116*, 1958.
20. Zhang, S.; Minus, M. L.; Zhu, L.; Wong, C. P.; Kumar, S. *Polymer* **2008**, *49*, 1356.
21. Ning, N.; Deng, H.; Luo, F.; Wang, K.; Zhang, Q.; Chen, F.; Fu, Q. *Compos. B* **2011**, *42*, 631.
22. Ning, N.; Luo, F.; Wang, K.; Du, R.; Zhang, Q.; Chen, F.; Fu, Q. *Polymer* **2009**, *50*, 3851.
23. Baer, E.; Hiltner, A.; Keith, H. D. *Science* **1987**, *235*, 1015.
24. Jarus, D.; Hiltner, A.; Baer, E. *Polym. Eng. Sci.* **2001**, *41*, 2162.
25. Mueller, C.; Topolkaraev, V.; Soerens, D.; Hiltner, A.; Baer, E. *J. Appl. Polym. Sci.* **2000**, *78*, 816.
26. Wang, H.; Keum, J. K.; Hiltner, A.; Baer, E.; Freeman, B.; Rozanski, A.; Galeski, A. *Science* **2009**, *323*, 757.
27. Wang, H.; Keum, J. K.; Hiltner, A.; Baer, E. *Macromolecules* **2010**, *43*, 3359.
28. Ponting, M.; Lin, Y.; Keum, J. K.; Hiltner, A.; Baer, E. *Macromolecules* **2010**, *43*, 8619.
29. Turner-Jones, A.; Aizlewood, J. M.; Beckelt, D. R. *Makromol. Chem.* **1964**, *75*, 134.
30. Olley, R. H.; Bassett, D. C. *Polymer* **1982**, *23*, 1707.
31. Yang, K.; Yang, Q.; Li, G.; Sun, Y.; Feng, D. *Mater. Lett.* **2006**, *6*, 805.
32. Wang, Y.; Shen, H.; Li, G.; Mai, K. *J. Therm. Anal. Calorim.* **2010**, *99*, 399.
33. Nakamura, K.; Shimizu, S.; Umemoto, S.; Thierry, A.; Lotz, B.; Okui, N. *Polym. J.* **2008**, *40*, 915.
34. Labour, T.; Cauthier, C.; Séguéla, R.; Vigier, G.; Bomal, Y.; Orange, G. *Polymer* **2011**, *42*, 7127.
35. Su, Z. Q.; Chen, X. N.; Yu, Z. Z.; Zhang, L. *J. Appl. Polym. Sci.* **2009**, *111*, 786.
36. Su, Z. Q.; Dong, M.; Guo, Z. X.; Yu, J. *Macromolecules* **2007**, *40*, 4217.
37. Dong, M.; Guo, Z. X.; Su, Z. Q.; Yu, J. *J. Appl. Polym. Sci.* **2011**, *119*, 1374.
38. Dong, M.; Guo, Z. X.; Yu, J.; Su, Z. Q. *J. Polym. Sci. Part B: Polym. Phys.* **2009**, *47*, 314.
39. Dong, M.; Guo, Z. X.; Yu, J.; Su, Z. Q. *J. Polym. Sci. Part B: Polym. Phys.* **2008**, *46*, 1725.
40. Dong, M.; Guo, Z. X.; Su, Z. Q.; Yu, J. *J. Polym. Sci. Part B: Polym. Phys.* **2008**, *46*, 1183.
41. Varga, J. *J. Macromol. Sci. Phys.* **2002**, *41*, 1121.
42. Varga, J.; Ehrenstein, M. *J. Therm. Anal. Calorim.* **1999**, *56*, 1047.
43. Varga, J.; Menyhárd, A. *Macromolecules* **2007**, *40*, 2422.
44. Wang, S.; Yang, W.; Bao, R.; Wang, B.; Xie, B.; Yang, M. *Colloid Polym. Sci.* **2010**, *288*, 681.
45. Norton, D. R.; Keller, A. *Polymer* **1985**, *26*, 704.
46. Li, H.; Jiang, S.; Wang, J.; Wang, D.; Yan, S. *Macromolecules* **2003**, *36*,2802.
47. Li, H.; Zhang, X.; Kuang, X.; Wang, J.; Wang, D.; Li, L.; Yan, S. *Macromolecules* **2004**, *37*, 2847.
48. Sun, X.; Li, H.; Wang, J.; Yan, S. *Macromolecules* **2006**, *39*, 8720.
49. Varga, J.; Karger-Kocsis, J. *J. Polym. Sci. Part B: Polym. Phys.* **1996**, *34*, 657.
50. Varga, J.; Ehrenstein, G. W. *Polymer* **1996**, *37*, 5959.
51. Hong, K.; Strobl, G. *Macromolecules* **2006**, *39*, 268.